

# Investigations of the emission geometry of the four-component radio pulsar J0631+1036

Mateus M. Teixeira,<sup>1</sup> Joanna M. Rankin,<sup>1,3★</sup> Geoffrey A. E. Wright<sup>2,3</sup> and J. Dyks<sup>4</sup>

<sup>1</sup>*Department of Physics, University of Vermont, Burlington, VT 05405, USA*

<sup>2</sup>*Astronomy Centre, University of Sussex, Falmer BN1 9QJ, UK*

<sup>3</sup>*Astronomical Institute ‘Anton Pannekoek’, University of Amsterdam, Science Park 904, 1098 XH Amsterdam, the Netherlands*

<sup>4</sup>*Nicolaus Copernicus Astronomical Center, Radańska 8, PL-87-100 Toruń, Poland*

Accepted 2015 October 27. Received 2015 September 29; in original form 2014 April 11

## ABSTRACT

Radio pulsar J0631+1036 presents a remarkably clear example of a rare four-component profile, and with apparently large aberration/retardation indicated by its linear polarization-angle traverse, but on closer study its profiles are somewhat difficult to understand and interpret. The pulsar’s four components do appear to represent inner and outer conal beam pairs with the expected spacing and spectral evolution with frequency. At metre wavelengths, the leading and trailing component pairs are often conflated into an unresolved double form by what seems to be varying amounts of scattering. We assess whether the core/double-cone geometric model, widely used to describe the profiles of slower pulsars, is appropriate for J0631+1036. We find that it is largely compatible apart from difficulties with the emission height and resolved double form of the inner conal features. An aberration/retardation analysis provides 600-km physical emission height values, which are compatible with geometric estimates for the outer conal emission. We also explore several other models and conclude that none are as successful as the core/double-cone model despite its several difficulties.

**Key words:** polarization – radiation mechanisms: non-thermal – pulsars: general – pulsars: individual (J0631+1036).

## 1 INTRODUCTION

The very unusual pulse profile of pulsar J0631+1036 in Fig. 1 (top) consists of two pairs of nearly symmetrical components, all highly linearly polarized at higher frequencies. Four-component forms are rare in the radio pulsar population, whereas one finds hundreds of triple and scores of five-component profiles. For slower pulsars (rotation periods greater than 100 ms or so), the core–double-cone beaming model provides a successful quantitative description for the vast majority of stars (e.g. ‘Empirical Theory’ series VI, Rankin 1993a,b; Mitra & Rankin 2010, ET IX). Triple profiles then usually represent sightline traverses through one cone and the core, whereas five-component profiles reflect both cones and the core. The few known four-component profiles exhibit forms similar to those of five-component pulsars – but absent a central core feature owing either to weakness or to a sightline that just misses it (e.g. B1738–08 in ET VI) – either case resulting in significant emission at the profile centre. Also the inner conal component pair is generally weaker with a flatter spectrum. Thus, these four components do not appear evenly spaced – but rather as clear leading and trailing

pairs. The J0631+1036 21-cm profile is thus noteworthy on all these grounds: the near even spacing of its four features, the deep central emission minimum, and the relative weakness of its outer component pair.

This is not all: the fractional linear polarization of the high-frequency profiles in Fig. 1 is unusually complete across almost their full widths. Further, the accompanying polarization position angle (hereafter PPA) traverse of J0631+1036 is no less remarkable, sweeping the greater part of the canonical 180° associated with a central sightline geometry, but in a highly asymmetric manner. Indeed, the steepest gradient (SG) point falls not near the profile centre but on its far trailing edge, clearly suggesting that aberration/retardation (hereafter A/R) is a significant factor in its structure.

PSR J0631+1036 was discovered by Zepka et al. (1996). It has a rotation period  $P$  of 0.288 s and a spindown of  $1.05 \times 10^{-13}$  s s<sup>-1</sup>, giving it a large magnetic field ( $5.6 \times 10^{12}$  G), acceleration potential across the polar cap ( $67 \times 10^{12}$  V) and rotational energy loss rate ( $1.7 \times 10^{35}$  erg s<sup>-1</sup>). The pulsar was also detected at  $\gamma$ -ray energies by the Fermi-LAT Observatory (Weltevrede et al. 2010), and Seyffert et al. (2011) further discuss its interpretation. Such a high energy-loss rate and acceleration potential suggest that its radio emission might well be core dominated, but nothing about its profile form supports this. This pulsar also has unusually high

\* E-mail: [Joanna.Rankin@uvm.edu](mailto:Joanna.Rankin@uvm.edu)

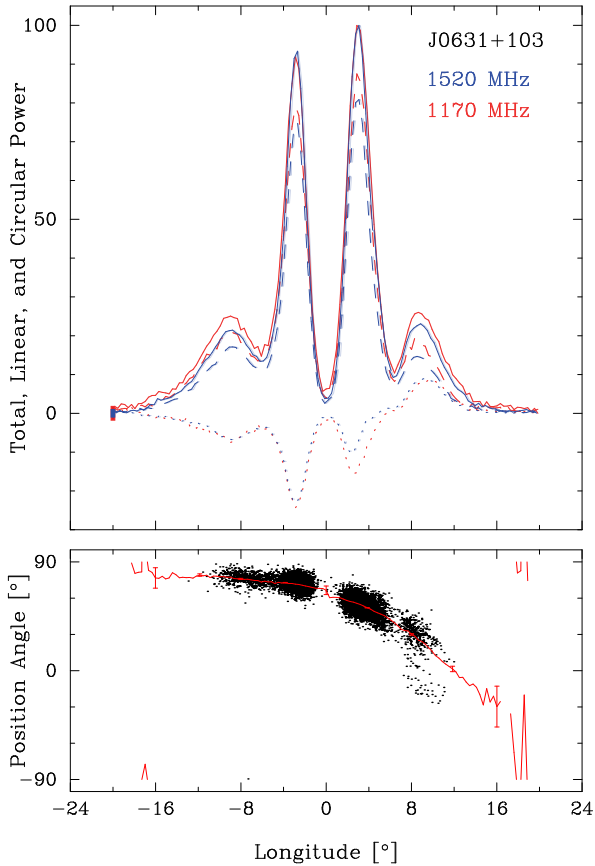


**Figure 1.** Overlaid average profiles at 1170 MHz (red) and 1520 MHz (blue), including polarimetry information (Stokes  $I$ , solid curve; linear  $[\sqrt{Q^2 + U^2}]$  dashed; and circular  $V$  dotted), for pulsar J0631+1036 on MJD 54540 scaled to an arbitrary intensity maximum. The average PPA  $[\frac{1}{2} \tan^{-1} U/Q]$  traverse in the bottom panel corresponds to that of the three combined bands. The error box at the left shows the resolution as well as three standard deviations in the off-pulse noise level.

dispersion (DM) and rotation measures for its position near the Galactic anticentre, and Zepka et al. (1996) speculate that it may be interacting with a relatively dense environment which is not its supernova remnant of birth.

Finally, the pulsar’s evolution with frequency has been difficult to understand. At 430 MHz in Zepka et al.’s fig. 3, the J0631+1036 profile is much broader and has an unresolved double form. Such a profile evolution – that is, broader at longer wavelengths – is an expected aspect of outer conal emission; however, that the apparent change from four to two components deserves explanation.

This report draws on some new Arecibo observations as described in Table 1. Section 2 then presents the new observations and their geometric analyses. Section 3 discusses the implications of this geometry theoretically. Section 4 presents different possible emission models, and Section 5 provides an overall summary and discussion.

## 2 DOUBLE-CONE/CORE BEAM MODEL

### 2.1 Morphology and conal spreading

In order to resolve these issues, we carried out Arecibo polarimetry observations at three bands in close succession on the same days as indicated in Table 1. Two profiles from the MJD 56514 observation are shown in Fig. 2 [and are aligned using Weltevrede et al.’s (2010)

**Table 1.** Arecibo polarimetry observations.

Band	MJD Date	BW/chans (MHz)	Resolution (°)	Length (min)
P	54016	25/256	2.81	20
L	2006 Oct 8			
L	54540	300/384	0.32	20
L	2008 Mar 15			
L	56500	258/384	0.70	10
U	2013 Jul 27	12/128	0.70	60
P		50/2048	1.41	60
L	56514	258/384	1.25	6.2
U	2013 Aug 10	22.7/1024	1.41	60
P		50/4096	1.41	47.3

*Notes.* Observations with centre frequencies of 327 MHz (P), 430 MHz (U) and 1170, 1420, and 1520 MHz (L) were carried out with the Wideband Arecibo Pulsar Processor before MJD 56000 (see Smith, Rankin & Mitra 2013 for observational details) and the Mock Spectrometers thereafter (e.g. Mitra, Arjunwadkar & Rankin 2015). Four bands of 86 (12.5) MHz centred at 1270, 1420, 1520, and 1620 MHz (308.25, 320.75, 333.25, 345.75) were used to cover the available L (P) receiver bands.

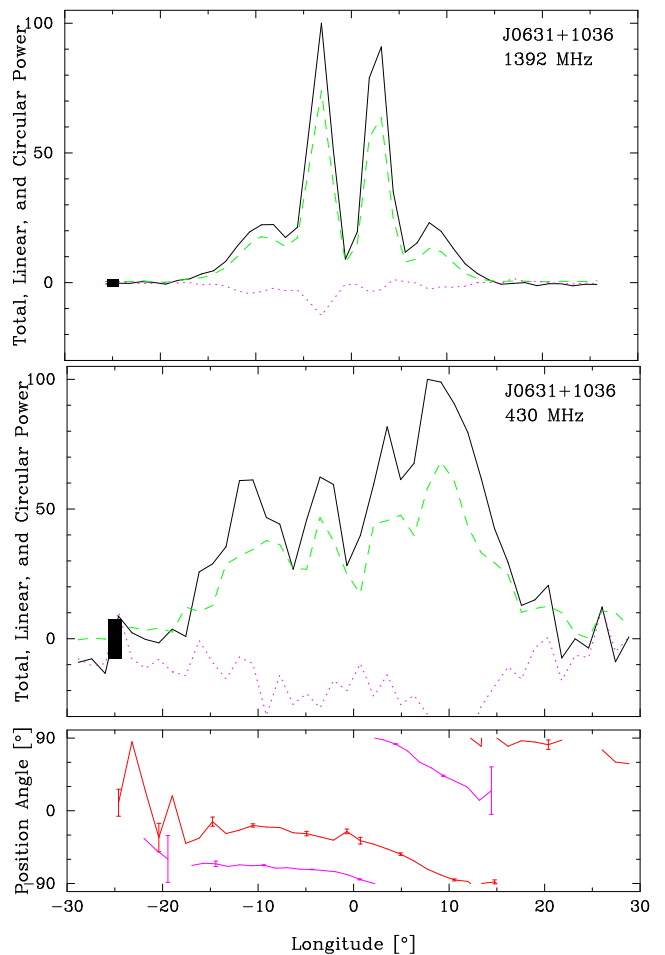


**Figure 2.** Time-aligned profiles corresponding to two of the three bands observed on MJD 56514: 1392 (top) and 430 MHz (middle, with the respective PPA curves just below). The star’s four components show clearly in this 430-MHz profile. Note that despite its larger width, the inner cone spacing is identical to that at 1.4 GHz and the outer cone only  $2^\circ$ – $4^\circ$  wider.

**Table 2.** Double-cone geometry model for PSR J0631+1036.

Freq (MHz)	$w_i$ ( $^\circ$ )	$\rho_i$ ( $^\circ$ )	$w_o$ ( $^\circ$ )	$\rho_o$ ( $^\circ$ )	$h_i$ (km)	$h_o$ (km)
2380	8.3	7.3	21.0	10.3	103	204
1665	8.3	7.3	21.5	10.4	103	209
1520	8.3	7.3	22.0	10.6	103	215
1420	8.3	7.3	22.5	10.7	103	221
1170	8.3	7.3	23.2	10.9	103	230
430	$\sim 9$	$\sim 7.5$	$< 33$	$< 13.4$	$\sim 107$	$< 343$
327	–	–	$< 34$	$< 14.4$	–	$< 395$

Notes.  $w_i$  and  $w_o$  are the outside half-power widths of the putative inner and outer cones (measured to about  $0^\circ.1$ ), respectively, as are  $\rho_i$ ,  $\rho_o$  and  $h_i$ ,  $h_o$  the corresponding beam radii and characteristic emission heights (errors typically 1 per cent) per the conventions of ET VI.  $\alpha$  is taken as  $52^\circ$  and  $\beta$  as  $-6^\circ.7$ , such that  $R_{PA} [= \sin \alpha / \sin \beta]$  is  $-6.8 \text{ deg deg}^{-1}$ .

DM value of  $125.36 \text{ pc cm}^{-3}$  and Yuan et al.'s (2010) timing solution]. The 430-MHz profile (lower panel) is better resolved than Zepka et al.'s and shows fourfold structure corresponding to the four features at 1.4 GHz (top panel).

These profiles then resolve the mysteries about J0631+1036's profile evolution: the outer conal component pair strengthens relative to the inner one with wavelength, so that at metre wavelengths both pairs have comparable intensities – a trend that was discernible even in Fig. 1 and the Zepka et al. profiles. The 327-MHz profile (not shown), however, has only an unresolved double structure. Thus, the fourfold structure at 327 MHz (and at times at 430 MHz) seems to be conflated by scattering.

This scattering appears to be variable from day to day. The four components of the 430-MHz profile of Fig. 2 are well resolved; however, a similar observation two weeks earlier showed only a rough double form similar to another 327-MHz profile from MJD 54016. The unshown 327-MHz profile corresponding to those in Fig. 2 showed only moderate linear polarization which was uniform across the profile, whereas other 327-MHz profiles have a highly polarized leading region and a depolarized trailing one with a flattened PPA traverse. The varying forms of our low-frequency profiles in breadth, depolarization, and trailing-edge flattening of the PPA traverse (at 430 MHz as well) then to confirm that the above authors were correct in attributing the low-frequency broadening to scattering.

The full width at half-maximum (FWHM) width for the 1520-MHz total power profile – here following the procedures of ET VI in using the outside half-power points of the putative outer conal component pair – is some  $22^\circ.5$ . By using our other profiles similarly at 1170 and 1420 MHz and those of Zepka et al. at 1665 and 2380 MHz (all with errors of  $\pm 0^\circ.1$ ), we assemble the widths for modelling in Table 2, where we see the expected outer conal increases with wavelength due to ‘radius-to-frequency mapping’. The lower frequency outside widths are significantly broader, whereas the 430-MHz peak spacing in Fig. 2 seems to change little; therefore, the increase is due more to scattering.

FWHM values for the inner component pair, by contrast, change little with frequency as is expected for an inner cone, hovering around  $8^\circ.3 \pm 0^\circ.1$  to perhaps  $9^\circ$  at 430 MHz. Moreover, the inner conal component pair weakens with wavelength relative to the outer pair, again a typical behaviour in double-cone profiles.

A rotating-vector-model (RVM) fit to the pulsar's PPA traverse at 1520 MHz in Fig. 1 was computed. The four-parameter fit confirms that the SG point falls near  $+9^\circ.7$ , perhaps with a  $\pm 1^\circ$  uncertainty in view of its correlation with other parameters. It also determines

**Table 3.** Aberration/retardation results for PSR J0631+1036.

$\phi_l$ ( $^\circ$ )	$\phi_t$ ( $^\circ$ )	$\nu$ ( $^\circ$ )	$\rho$ ( $^\circ$ )	$r_{em}$ (km)	$s_L$
Outer cone					
-20.8	+1.3	-9.8	10.6	585	0.60
(0.2)	(0.2)	(0.14)	(0.1)	(8)	(0.01)
Inner cone					
-13.6	-5.4	-9.5	7.4	570	0.42
(0.1)	(0.1)	(0.07)	(0.03)	(4)	(0.01)

Note:  $\phi_l$  and  $\phi_t$  are the respective leading and trailing component positions and  $\nu$  their difference.  $\rho$  is the conal radius,  $r_{em}$  the A/R-estimated physical height, and  $s_L$  the fractional annulus on the polar cap. The A/R height values do not depend on the emission geometry, but the conal and ‘footprint’ radii do. The  $\alpha$  and  $\beta$  values are taken as in Table 2.

nominal values of the magnetic colatitude  $\alpha$  and sightline impact angle  $\beta$ . However, these latter values are typically 99 per cent correlated, so it is the PPA slope  $R_{PA} [= \sin \alpha / \sin \beta]$  at the SG point that is significant and well determined (see also ET IX). This value is  $-6.8 \pm 0.2 \text{ deg deg}^{-1}$ .

## 2.2 A/R emission height estimation

As we saw in the J0631+1036 profiles above, the star's PPA traverse is so SVM-like and its SG point so delayed with respect to the profile centre that the situation seems to demand A/R analysis. Not so fast, however! The physical basis and practical application of A/R analysis was first developed by Blaskiewicz, Cordes & Wasserman (1991), but only over the last decade or so has it found wide application and provided increasingly consistent results. Fundamental to all A/R analyses is reliable determination of a profile centre which can be interpreted as the longitude of the magnetic axis. Such interpretations have followed one of two courses: (a) taking the mid-point between two conal components relative to the PPA SG point as falling symmetrically on either side of the magnetic axis longitude or (b) taking the centre of a core component as marking the magnetic axis longitude (Malov & Suleymanova 1998).

Pulsar J0631+1036's unusual profile above, however, has given us pause. We have found strong evidence above that the star's four components represent inner and outer conal component pairs. Given their high symmetry – as well as the strong asymmetry of the PPA traverse – it is hard to understand how the longitude of the magnetic axis could fall at any point other than mid-way between the conal component pair centres and the PPA SG point.

So emboldened, we have conducted an A/R analysis of the former type. However, in terms of computations, all are the same, and the values in Table 3 are similar to tables in previous such efforts in Srostlik & Rankin (2005), Force & Rankin (2010), or ET IX and are corrected as advised by Dyks, Rudak & Harding (2004).  $\phi_l^i$  and  $\phi_t^i$  are the respective leading and trailing longitudes of the centres of one or the other component pairs;  $\nu^i$  is the computed centre of the pair;  $\rho^i$  is the computed radius of the emission cone; and  $r_{em}^i$  and  $s_L^i$  give the physical emission height and relative polar cap annulus, respectively.

## 2.3 Quantitative geometry

The most accurate and consistent estimates of a radio pulsar's emission geometry – that is, its magnetic colatitude  $\alpha$  and sightline impact angle  $\beta$  – result from using *both* the angular width information of its profile and the sightline path information in its PPA

traverse. This was the method used in ET VI (Rankin 1993) wherein the bulk of the population with the well-measured polarization profiles was found to exhibit a core and double-cone structure – that is, with a half-power core width of  $2.45P^{-1/2}$  and outside half-power conal radii of  $4.3P^{-1/2}$  and  $5.8P^{-1/2}$  (all at 1 GHz), respectively.<sup>1</sup> And these conal radii then imply *characteristic* emission heights of some 130 and 220 km, respectively.<sup>2</sup>

Pulsar J0631+1036's profile had seemed so unusual that we were slow to assess whether it might represent an inner and outer conal component pair. However, as we have seen in the foregoing sections, the actual properties of its profile largely appear compatible with this interpretation. Here we ask whether such a geometry is consistent quantitatively. No core feature is discernible at any frequency for this pulsar, so we have no independent means of estimating the pulsar's magnetic colatitude  $\alpha$ . However, we can ask whether there is an  $\alpha$  value such that the two emission cones have their expected dimensions.

Table 2 gives such a double-cone geometric model for J0631+1036. The model values of  $\alpha$  and  $\beta$  are  $52^\circ$  and  $-6.7^\circ$ , such that the PPA sweep rate  $R_{\text{PPA}}$  is  $-6.8 \text{ deg deg}^{-1}$  as determined by the above PPA fit. The respective inner and outer conal radii are computed according to ET VI equation (4) and the emission heights per equation (6). Only for this last computation is the pulsar's rotation period  $P$  (0.288 s) used to estimate the angular size of the star's polar cap so that magnetic-polar colatitudes can be related to *characteristic* emission heights.

Reasonable conal dimensions and characteristic heights are obtained using the model in Table 2 for  $\alpha$  values between about  $50^\circ$  and  $60^\circ$ . For  $\alpha$  near the upper value, the inner cone exhibits its expected radius and height, and for the lower value the outer cone assumes a radius such that the model 1-GHz *characteristic* emission height is about the expected 220 km. That the model fails to indicate a unique  $\alpha$  value is unusual – and here minor – and otherwise the model is not unsatisfactory.

### 3 GEOMETRY OF NESTED CONES

Here we explore geometrically the nested-cone structure inferred for this pulsar: the roughly equal distances between components ( $\Delta \approx 6^\circ$ ) and near-zero flux at the centre constrain the double-cone geometry strongly.

In the plane geometry of Fig. 3, the two semicircles represent the maxima of the emission cones,  $\kappa$  their ratio  $\rho_1/\rho_2$  (shown here as 0.74), and  $\Delta$  is the separation between the profile peaks along the sightline. Two Pythagorean theorems can be written for the two right triangles:  $(\rho_1, \Delta/2, \beta)$  and  $(\rho_2, 3\Delta/2, \beta)$ , and solved for  $\Delta$  and  $\beta$ . These are  $|\Delta|/(\rho_1) = [(1 - \kappa^2)/2\kappa^2]^{1/2}$  and  $|\beta|/\rho_1 = [(9\kappa^2 - 1)/8\kappa^2]^{1/2}$ , respectively.

The two quantities depend only on the ratio  $\kappa$  of the cones' size. In the spherical case, the latter equation has two solutions for  $\rho_1$ , and positive and negative solutions for  $\beta$ . Numerical solution of the spherical geometry shows that it remains fully valid. Thus,  $\beta$  and

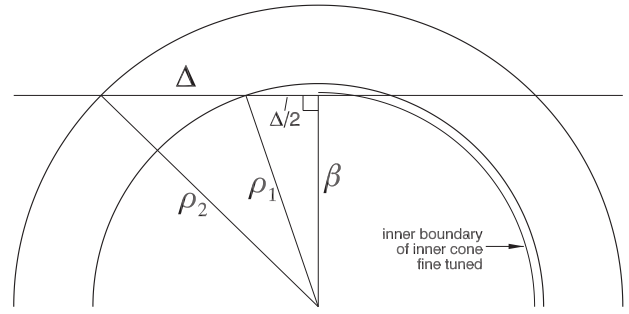


**Figure 3.** Viewing geometry for a double-cone profile with four equidistant components and the frequently observed cone-size ratio  $\kappa = \rho_1/\rho_2$  of 0.74. The sightline, impact angle  $\beta$ , and separation  $\Delta$  are marked.

$\rho_1$  scale as in the latter relation, with no other dependence on  $\alpha$  or  $\Delta$ .

As can be seen in the nested cone model of Fig. 3, doubly fine-tuned conditions are needed to generate a profile with equidistant components and a deep central minimum. First, for a reasonable cone-size ratio ( $\kappa \gtrsim 0.5$ ) the impact angle  $\beta$  must be a precise fraction of  $\rho_1$ . Since  $\beta/\rho_1$  changes very slowly with  $\kappa$  (for  $\kappa \gtrsim 0.5$ ), even a small mistuning in  $\beta$  does not result in the equidistance. Secondly, to produce the equidistance, the sightline must almost be grazing the very edge of the inner cone. Wright (2003) has argued that both observational (ET VI) and theoretical arguments support the value  $\kappa = 0.74$ , for which  $\beta/\rho_1 = 0.95$ . Thus, for the cone ratio typically found in statistical studies, the sightline would pass tangentially across the inner cone edge, just crossing the radial peak. Then, a well-resolved inner cone double form requires that its inner boundary be very close to its peak (as shown in Fig. 3) – implying a further level of fine-tuning to reproduce the low flux at the profile centre. The situation does not much improve  $\kappa = 0.5$ , because  $\beta/\rho_1 = 0.79$  is still quite large.

In short, the double-cone model with circular beams has to be unacceptably fine-tuned to describe J0631+1036's profile, and the problem is not unique to it but arises for other pulsars with similar geometries as well. This small group shows clearly that the double-cone model with circular beams requires modification under these conditions, but observations give little guidance about just what is required.

## 4 ALTERNATIVE EMISSION MODELS

### 4.1 Conal downflow models

We first examined a model wherein some of the profile components of J0631+1036 were generated by radiation from downflowing particles on the far side of the pulsar. Downflow models have occasionally been invoked (e.g. in B1822–09, Dyks, Zhang & Gil 2005) but have not been convincing. Nevertheless, radius-to-frequency mapping – which seems to be observed in many pulsars – might naturally account for J0631+1036's near-symmetric profile. Two components might then stem from nearside emission and two from the farside and then two configurations are possible: either components 1 and 3 are a nearside cone (and 2 and 4 stem from farside downward emission) or components 1 and 2 are the nearside cone (with 3 and 4 from the farside). Although these models led to not unreasonable emission heights, the generated PPA swings failed to yield SGs at the observed position on the far trailing profile edge. The symmetric pattern of component thickness was also lost.

<sup>1</sup> Lyne & Manchester (1988) carried out a similar geometric study and came to many similar conclusions.

<sup>2</sup> Such *characteristic* emission heights are not to be confused with actual, physical emission heights. In the ET VI context, computation of emission heights entails association of the conal emission outer boundary (for both inner and outer cones!) with the 'last open' field line. Clearly this is implausible physically; its use, however, provides a consistent outer boundary for emission along the edges of the polar flux tube.

Further, we supposed that the outer components arise from identical single beams at either pole, each forming a narrow axisymmetric cone about the pulsar's magnetic axis. Then the outer components of J0631+1036 are the frequency-dependent manifestation of the upward nearside and downward farside emission at a particular height, and our sightline comes closest to the magnetic axes at this height at the component centres. The inner components might then arise as caustic effects, so that intrinsically weak emission is boosted to detectable levels by the geometric coincidence of our sightline moving instantaneously parallel to the trajectory of the emitting particles (see Dyks, Wright & Demorest 2010b). This model identified the fiducial point naturally as a deep minimum (as observed) and yielded the sequence of component sizes at plausible heights, but it required that the SG position be determined entirely by the nearside emission. This weakness, together with its unprecedented reliance on caustic emission, failed to be convincing.

## 5 SUMMARY AND DISCUSSION

Pulsar J0631+1036 provides an unusually good example of a pulsar with a four-component profile. Radio pulsars with four components are rare, so it is important to understand its beam form geometry and emission heights. Observationally, we are able to conclude the following.

- (i) J0631+1036's four emission components evolve as two pairs, an inner and outer one.
- (ii) The inner pair has a somewhat flatter spectrum and a spacing which is nearly constant over the range of our observations – as expected for inner cones. At metre wavelengths, the two pairs have comparable intensities, whereas the inner pair is stronger at higher frequencies.
- (iii) The outer pair exhibits a modest increase in spacing with wavelength – as is expected for outer cones.
- (iv) At metre wavelengths, the four components are often conflated by scattering into a leading and trailing 'hump' – giving these profiles an unresolved double form. The scattering appears to be temporally variable.
- (v) The linear polarization is unusually high but not complete at all frequencies.
- (vi) The SG point of the PPA traverse has a well determined slope of  $-6.8 \pm 0.2^\circ$  and falls near longitude  $+9^\circ 7'$  under the trailing component

We found it challenging to accommodate all these properties comfortably within the double-cone model of radio pulsar emission geometry. However, assuming this configuration,

- (i) the A/R analysis in Table 3 gives plausible 600-km physical emission heights for both cones, but most earlier work suggests a lower emission height for the inner cone;
- (ii) the quantitative geometrical model in Table 2 accommodates the profile dimensions in a manner very like the double-cone pulsars studied in ET VI for  $\alpha$  values of between  $50^\circ$  and  $60^\circ$  – that is, with the usual inner and outer conal beam radii scaled to the angular size of the pulsar's polar cap;
- (iii) the outer cone characteristic emission height of just some 220 km is compatible with the A/R physical height above, being about 2.5–3 times smaller;
- (iv) the inner cone height is not only somewhat smaller than the usual 125 km found in ET VI, but it is much smaller than would be expected from the A/R analyses;

- (v) the nearly equal spacing of the components and nearly zero flux at the centre of the profile are difficult to understand if the conal beams are circular.

The latter is a major problem. Some elliptical extension of the beams in latitude may help resolve this difficulty, as has been proposed to account for the precessing beams of B1913+16 and J0737–3039B (Weisberg & Taylor 2002; Clifton & Weisberg 2008; Perera et al. 2010). It is also possible that some beam modification occurs for emission at higher altitudes or in pulsars with large spindown torques.

Most double-cone profiles exhibit a core component, but we see no core feature in J0631+1036. However, it may not be discernible because it is conflated with other emission. If the above geometry is correct, there are at least two reasons why no core component is seen in the profile: (a) the radius of the core beam would be some  $2:3$ , whereas  $\beta$  is some  $-6:7$ , so that bivariate-von Mises-shaped core-beam power would be attenuated by a factor of about 20; and (b) what power remains would appear not in the empty profile region between the two inner conal components, but rather half-way between this point and the PPA SG point, at some  $+4^\circ 8'$  longitude in Fig. 1, where it would be conflated with power from the trailing inner conal component.

The Gil & Sendyk (2000) model gives some added flexibility (though most double cones appear to stem from a single ring of 'sparks'). However, in the case of J0631+1036 we find that the required double-cone geometry needs to be so contrived as to be implausible. Invoking emission from particle downflow from the farside of the pulsar (Section 4) resolves some of the geometric issues but at the price of becoming physically implausible.

A further alternative approach, which we did not examine here are the 'wedge' or 'fan' models (Dyks, Rudak & Demorest 2010a; Wang et al. 2014; Dyks & Rudak 2015). These profile models entail fixed streams of emission azimuthally arranged around the magnetic pole. The models do not presuppose any specific polar cap physics, nor any prescribed frequency distribution within their streams, and this gives them great flexibility. They also differ in that they have little to say about single-pulse behaviour, which is not immediately of issue here.

Such models support a view that some multi-peaked profiles result from line-of-sight intersections across spokes of fixed emission wheels centred on the magnetic pole. J0631+1036 would then owe its dramatic profile partly to chance alignment of the wheel and partly to the highly oblique line of sight. The fan model has had some successes so far (e.g. Desvignes et al. 2012). However, its great flexibility comes at the high cost of physical arbitrariness. As pointed out by Dyks & Rudak (2015), a range of pulsars need be explained in single-pulse detail before such models can claim any significant physical foundation.

The highly symmetrical profile of J0631+1036 then strongly suggests a double-cone structure as in ET VI, but careful application of the model encounters several kinds of difficulties as outlined above. These difficulties may stem from the unusually large spindown energy and torque as exemplified by its prominently delayed PPA SG point and  $\gamma$ -ray luminosity. However, we have not been able to clarify concretely how such distortions would arise physically.

## ACKNOWLEDGEMENTS

The authors thank the many colleagues who responded to our challenge to consider the issues that pulsar J0631+1036 raises and have thus contributed to the discussions above. We also thank

Dipanjana Mitra for adapting the RVM fitting software. GAEW thanks the Universities of Sussex and Manchester for Visiting Fellowships, and the Nederlandse Organisatie voor Wetenschappelijk Onderzoek (NWO) for a Visitor Bursary held at the 'Anton Pannekoek' Astronomy Institute (API) of the University of Amsterdam. Portions of this work were carried out with support from US NSF Grant AST 08-07691. Another part was supported by Polish National Science Centre grant DEC-2011/02/A/ST9/00256. Arecibo Observatory is operated by SRI International under a cooperative agreement with the US NSF, in alliance with Ana G. Mndez-Universidad Metropolitana, and the Universities Space Research Association. This work used the NASA ADS system.

## REFERENCES

- Blaskiewicz M., Cordes J. M., Wasserman I., 1991, *ApJ*, 370, 643  
 Clifton T., Weisberg J. M., 2008, *ApJ*, 679, 687  
 Desvignes G., Kramer M., Cognard I., Kasian L., van Leeuwen J., Stairs I., Theureau G., 2012, in van Leeuwen J., ed., *Proc. IAU Symp.* 291, Neutron Stars and Pulsars: Challenges and Opportunities after 80 years. Cambridge Univ. Press, Cambridge, p. 199  
 Dyks J., Rudak B., 2015, *MNRAS*, 446, 2505  
 Dyks J., Rudak B., Harding A., 2004, *ApJ*, 607, 939  
 Dyks J., Zhang B., Gil J., 2005, *ApJ*, 626, 45  
 Dyks J., Rudak B., Demorest P., 2010a, *MNRAS*, 401, 1781  
 Dyks J., Wright G. A. E., Demorest P., 2010b, *MNRAS*, 405, 509  
 Force M. M., Rankin J. M., 2010, *MNRAS*, 406, 237  
 Gil J., Sendyk M., 2000, *ApJ*, 541, 351  
 Lyne A. G., Manchester R. N., 1988, *MNRAS*, 234, 477  
 Malov I. F., Suleymanova S. A., 1998, *Astron. Rep.*, 42, 388  
 Mitra D., Rankin J. M., 2010, *ApJ*, 727, 92 (ET IX)  
 Mitra D., Arjunwadkar M., Rankin J. M., 2015, *ApJ*, 806, 236  
 Perera B. B. P. et al., 2010, *ApJ*, 721, 1193  
 Rankin J. M., 1993a, *A&AS*, 85, 145  
 Rankin J. M., 1993b, *ApJ*, 405, 285  
 Seyffert A. S., Venter C., de Jager O. C., Harding A. K., 2011, preprint ([arXiv:1105.4094v1](https://arxiv.org/abs/1105.4094v1))  
 Smith E., Rankin J., Mitra D., 2013, *MNRAS*, 435, 1984  
 Srostlik Z., Rankin J. M., 2005, *MNRAS*, 362, 1121  
 Wang H. G. et al., 2014, *ApJ*, 789, 1  
 Weisberg J. M., Taylor J. H., 2002, *ApJ*, 576, 942  
 Weltevrede P. et al., 2010, *ApJ*, 708, 1426  
 Wright G. A. E., 2003, *MNRAS*, 344, 1041  
 Yuan J. P., Wang N., Manchester R. N., Liu Z. Y., 2010, *MNRAS*, 404, 289.  
 Zepka A., Cordes J. M., Wasserman I., Lundgren S. C., 1996, *ApJ*, 456, 305

This paper has been typeset from a  $\text{\TeX}/\text{\LaTeX}$  file prepared by the author.